

Silicon photonic processor of two-qubit entangling quantum logic

R. Santagati,^{1,*} J. W. Silverstone,^{1,†} M. J. Strain,² M. Sorel,² S. Miki,³ T. Yamashita,³ M. Fujiwara,⁴ M. Sasaki,⁴ H. Terai,⁵ M. G. Tanner,² C. M. Natarajan,² R. H. Hadfield,² J. L. O'Brien,¹ and M. G. Thompson¹

¹*Quantum Engineering Technology Labs, H. H. Wills Physics Laboratory and Department of Electrical and Electronic Engineering, University of Bristol, BS8 1FD, UK.*

²*School of Engineering, James Watt South Building, University of Glasgow, Glasgow G12 8QQ, UK*

³*National Institute of Information and Communications Technology, 588-2 Iwaoka, Kobe 651-2492, Japan*

⁴*National Institute of Information and Communications Technology, 4-2-1 Nukui-Kitamachi, Koganei, Tokyo 184-8795, Japan*

⁵*National Institute of Information and Communications Technology, 588-2 Iwaoka, Kobe 651-2492, Japan*

Abstract: Entanglement is a fundamental property of quantum mechanics, and is a primary resource in quantum information systems. Its manipulation remains a central challenge in the development of quantum technology. In this work, we demonstrate a device which can generate, manipulate, and analyse two-qubit entangled states, using miniature and mass-manufacturable silicon photonics. By combining four photon-pair sources with a reconfigurable six-mode interferometer, embedding a switchable entangling gate, we generate two-qubit entangled states, manipulate their entanglement, and analyse them, all in the same silicon chip. Using quantum state tomography, we show how our source can produce a range of entangled and separable states, and how our switchable controlled-Z gate operates on them, entangling them or making them separable depending on its configuration.

I. INTRODUCTION

Photons remain a promising vehicle for the development of next-generation quantum technology [1, 2]. Integrated quantum photonics, with its intrinsic phase stability and miniature devices, is necessary to bring linear optics to the large scale [3–5]. Several integrated photonic platforms have emerged to solve this problem, including silica-on-silicon [3, 6–8], direct-write glass [9–13], lithium niobate [14–17], silicon nitride [18, 19] and silicon-on-insulator [20]. Silicon quantum photonics promises to simultaneously achieve the required functionality, performance, and scale.

Several important quantum optical functionalities have already been shown with high performance in silicon. Photon pairs can be generated using spontaneous four-wave mixing (SFWM) [21–26], and interfered with high visibility [26–30]. Single-photon [31] and pump-rejection [32, 33] spectral demultiplexers, as well as two-mode interferometers [34], have been demonstrated with very high extinction. Finally, single-photon detectors, based on superconducting nanowires have shown excellent performance on silicon waveguides [35, 36]. The very high refractive index contrast of silicon-on-insulator waveguides yields micron-scale components (e.g. [37]), while miniature ring resonator SFWM sources [22], and quantum interferometric networks [38] facilitate devices on a very large scale.

The integration of entangled qubit sources with entangling quantum logic, together on a common platform, is an important next step. Here we show a new method for generating path-encoded, variably entangled two-qubit states. We perform multi-qubit quantum logic on these states and study their entanglement. We implemented this scheme on a reconfigurable, silicon photonic device to generate a wide range of two-qubit states. We integrated this source with arbitrary state preparation, a switchable two-qubit gate, and an interferometer for tomographic analysis. The implemented quantum circuit is similar to the one reported in [39].

We tested the device's quantum logic capabilities with several experiments. We analysed the source performance using reversed-Hong-Ou-Mandel-type (RHOM) [28, 40] quantum interference, and qubit tomography on a wide range of possible states. We followed this with an exploration of the on-chip quantum logic, with the switchable two-qubit gate in both entangling ($\hat{C}Z$) and non-entangling (\hat{I}) configurations, and using the purity (P) [41], the CHSH parameter (S) [42] and the Schmidt number (K) [43] as diagnostic metrics.

II. DEVICE STRUCTURE AND OPERATION

A schematic of the device is shown in Figure 1a. It comprises a reconfigurable source of two path-encoded entangled photons, controlled by the parameters ϕ_β , ϕ_T and ϕ_B . The source is followed by a reconfigurable interferometer, able to implement any two-qubit projector (including entangled projections). This second part of the device can be divided into three sections: arbitrary single qubit gates, a switchable post-selected controlled-Z

* These authors contributed equally to this work.;
raffaele.santagati@bristol.ac.uk

† These authors contributed equally to this work.;
josh.silverstone@bristol.ac.uk

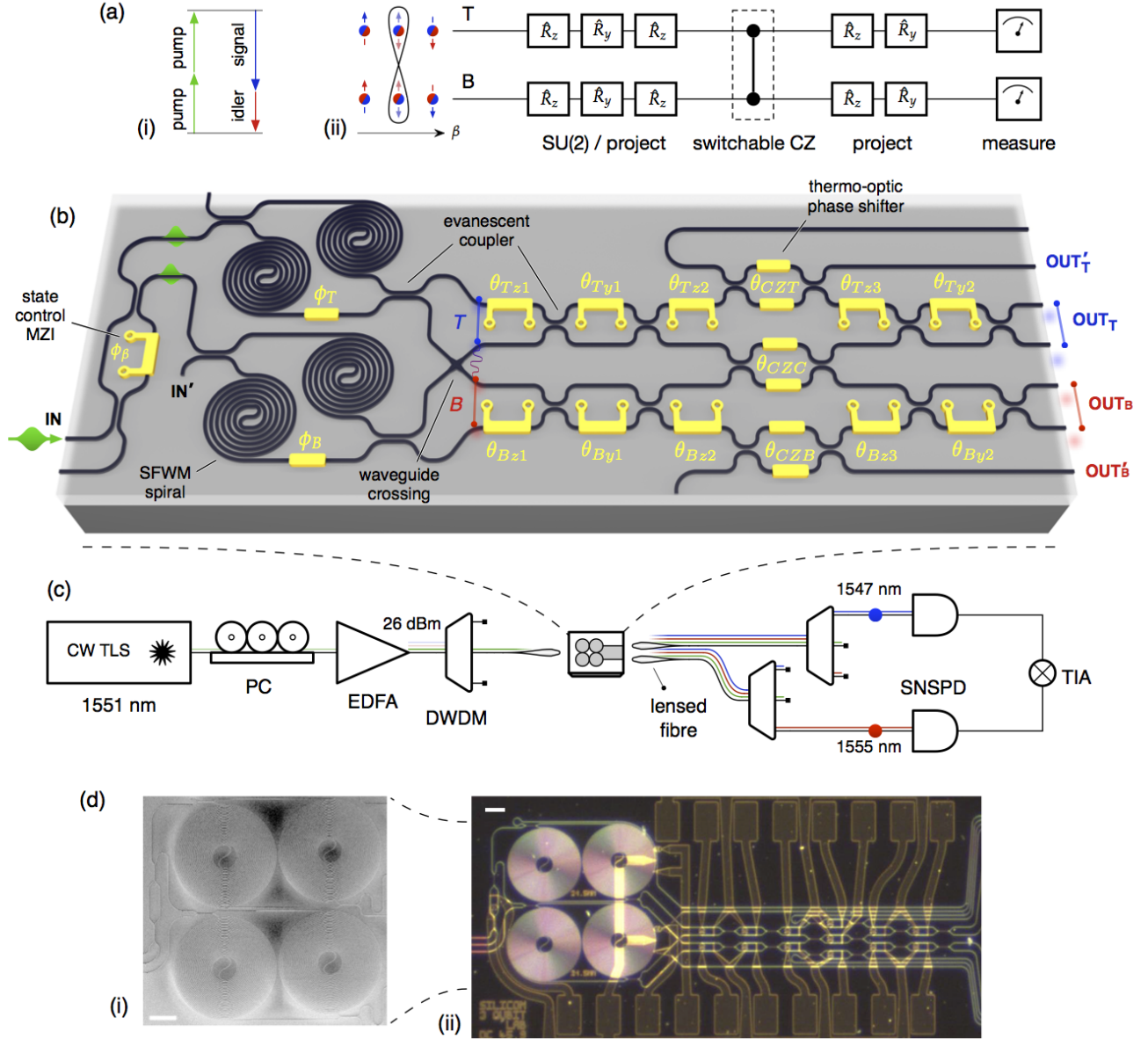


FIG. 1. Device and apparatus overview. **a** Operating principles. **i** Non-degenerate spontaneous four-wave mixing, **ii** quantum circuit description. **b** Schematic of the silicon quantum photonic chip. A pump laser is coupled into the device, coherently pumping two spiralled RHOM sources which produce two photons entangled or separable in path. These are fed into a reconfigurable linear optical network which can entangle or disentangle them, and analyse the output. **c** Off-chip apparatus. A continuous wave (CW) tunable laser source (TLS) is polarisation controlled (PC), amplified (EDFA), filtered and coupled onto the chip using lensed fibres and spot-size converters. Signal, idler, and pump photons coupled back into fibre in the same way, then spatially separated using dense wavelength-division multiplexers (DWDM), detected using superconducting nanowire single-photon detectors (SNSPD), and the output signal is analysed by a time interval analyser (TIA). **d** Electron **i** and optical **ii** micrographs of the device.

($\hat{C}z$ gate) gate [44], and final single-qubit unitaries, used to implement projectors for quantum state tomography, to reconstruct the output state.

The device comprised $500 \times 220 \text{ nm}^2$ waveguides, directional couplers (approximate length $45.9 \text{ }\mu\text{m}$), a waveguide crossing ($> 20 \text{ dB}$ isolation), and resistive metallic heaters (length $54.0 \text{ }\mu\text{m}$). It was coupled to fibre via edge coupling, fibre lenses, and polymer spot-size con-

verters. Electrical connections were achieved through multi-contact electrical probes and $200 - \mu\text{m}$ -pitch on-chip gold pads (approximately $120 \times 200 \text{ }\mu\text{m}^2$). Fabrication of the device proceeded as in reference [31].

The experimental setup is presented in Figure 1b. Photons are generated on the chip via SFWM, pumped by an amplified continuous-wave tunable laser, and filtered to remove in-band noise. An average facet-to-

facet transmission of ≈ -28 dB was observed. The dominant sources of loss were scattering at the chip facets, and propagation loss in the spiralled source waveguides. Inside the device the light was reconfigurably manipulated by an interferometric network, composed of evanescent coupler beam-splitters and thermo-optic phase-shifters [38, 45]. Photons were collected from the device, demultiplexed and separated from the pump using dense wavelength-division multiplexers (DWDM), detected using superconducting nanowire detectors [46], and finally converted into coincidence counts by a time-interval analyser.

A. Photon-pair generation

The strong non-linear properties of silicon waveguides are well known [47]. Spontaneous four-wave mixing (SFWM), an effect of the $\chi^{(3)}$ non-linearity, is now commonly used to produce photon pairs in silicon quantum photonic devices [21, 28].

In the non-degenerate SFWM process used here, two photons from a bright pump are annihilated, producing two correlated photons with different wavelengths (Figure 1a). The two generated photons, ‘signal’ and ‘idler’, emerge spectrally on either side of the pump, conserving energy and momentum. In our experiment, spiralled 21-mm-long waveguides were used to produce photon-pairs, with the pump, signal, and idler photon wavelengths being 1551 nm, 1547 nm, and 1555 nm. These photons were generated in a continuous spectrum and the chosen wavelengths were post-selected by the off-chip demultiplexers.

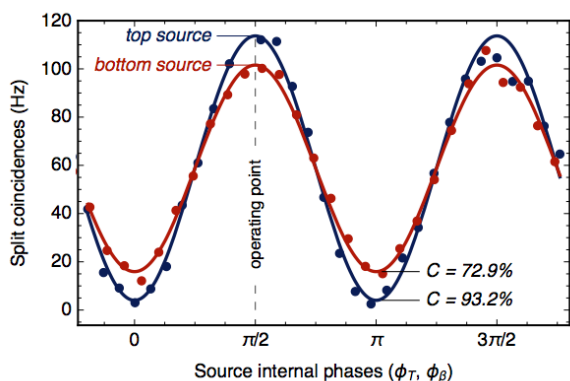


FIG. 2. Quantum interference for the two sources, measuring coincidences from the outputs OUT'_T and OUT'_B , obtained by pumping each RHOM source and scanning the source internal phase, ϕ_T or ϕ_B . The imperfect interference can be explained in terms of imbalance in the on-chip evanescent coupler beam splitters.

B. Entangled qubit generation

Our device uses a new scheme to generate entangled path-encoded states, which can subsequently be interfered, using pairs of *non-degenerate* photons. Pump laser is distributed between two reverse-HOM structures using a reconfigurable power splitter (splitting ratio $\sin^2[\phi_\beta/2]$). Each RHOM contains two spiralled waveguides and a thermal phase shifter, as in [28]. The internal RHOM phases (ϕ_T and ϕ_B) were set to $\pi/2$, such that the produced photon-pairs emerged deterministically split, one in each output waveguide, and in a state symmetrical between signal and idler photons. ϕ_β allows us to control the balance of photon-pair emission between the two RHOM structures, and so to control the entanglement present in the two-qubit output state.

Following Figure 1b, if $\phi_\beta = \pi$, photons will be generated only in the top RHOM, and the photon number output state, after the waveguide crossing, will be $|1010\rangle$, or $|00\rangle$ in the qubit basis. On the other hand, if $\phi_\beta = 0$, only the bottom RHOM generates photons, leading to $|0101\rangle = |11\rangle$. Finally, if $\phi_\beta = \pi/2$, we obtain the maximally entangled state: $|\Phi^\Theta\rangle \equiv (|00\rangle + e^{i\Theta}|11\rangle)/\sqrt{2}$, where Θ is a fixed phase factor due to the chip’s intrinsic path-length mismatch. Thus, the output state from the entangled qubit generator is

$$|\psi\rangle = \sqrt{\beta}|00\rangle + e^{i\Theta}\sqrt{1-\beta}|11\rangle \quad (1)$$

which can be continuously varied across a wide range of separable and entangled states, depending on the balance parameter, β . The balance depends on the square of the power division of the state control MZI (controlled by the phase ϕ_β), due to the two-photon dependence of SFWM:

$$\beta = \left| \frac{\sin^2(\phi_\beta/2)}{\sqrt{\sin^4(\phi_\beta/2) + \cos^4(\phi_\beta/2)}} \right|^2. \quad (2)$$

C. Quantum logic and analysis

The state $|\psi\rangle$ is fed into a two-qubit circuit, composed of single-qubit rotations, and a switchable entangling gate. We implemented the arbitrary rotations on each qubit by cascading phase-shifters and Mach-Zehnder interferometers (MZI). These were used to realise \hat{R}_z and \hat{R}_y rotations, respectively, obtaining an arbitrary $\text{SU}(2)$ with the combination $\hat{R}_z \cdot \hat{R}_y \cdot \hat{R}_z$.

We implemented a switchable entangling gate using a scheme based on [44], but replacing the 1/3 beam-splitters with tunable-reflectivity MZIs. In this way, we can switch the gate’s controlled-Z operation on and off. When on, the $\hat{C}z$ gate operation succeeds with probability 1/9. In the remaining 8/9 cases non-qubit states are generated, which are filtered by the coincidence-counting post-selection.

Source state	Gate	Purity P	Schmidt number K	CHSH S	Fidelity F'
$ 00\rangle$	bypassed	0.995 ± 0.012	1.012 ± 0.011	1.577 ± 0.072	0.973 ± 0.011
$ 00\rangle$	\hat{I}	0.946 ± 0.031	1.034 ± 0.017	1.465 ± 0.064	0.962 ± 0.016
$ 11\rangle$	bypassed	0.998 ± 0.008	1.004 ± 0.006	1.511 ± 0.049	0.984 ± 0.007
$ 11\rangle$	\hat{I}	0.949 ± 0.055	1.048 ± 0.037	1.601 ± 0.121	0.948 ± 0.031
$(00\rangle + 11\rangle)/\sqrt{2}$	bypassed	0.864 ± 0.019	1.905 ± 0.022	2.560 ± 0.037	0.909 ± 0.028
$(00\rangle + 11\rangle)/\sqrt{2}$	\hat{I}	0.832 ± 0.040	1.936 ± 0.025	2.538 ± 0.072	0.900 ± 0.026
$ ++\rangle$	$\hat{C}Z$	0.931 ± 0.036	1.657 ± 0.045	2.560 ± 0.078	0.873 ± 0.038
$(00\rangle + 11\rangle)/\sqrt{2}$	$\hat{C}Z$	0.900 ± 0.071	1.166 ± 0.055	1.907 ± 0.137	0.839 ± 0.013

TABLE I. Purity, Schmidt number, CHSH parameters and Fidelity for a variety of measured states. The Schmidt number and CHSH parameter indicate entanglement. $S > 2$ indicates the presence of non-local correlations [42], while K indicates the number of coefficients in the Schmidt decomposition of the state [43]. The fidelities F' reported are computed against the ideal state optimised over local R_z rotations, to compensate for the intrinsic random phase factor on each qubit.

Note that only the on ($\cos(\theta_{CZ}) = 1/3$) and off ($\cos(\theta_{CZ}) = -1$)

gate configurations produce unitary operations. The two qubit gate is followed by rotations (parametrised by $\theta_{Mz3}, \theta_{My2}, M \in \{T, B\}$) used to implement quantum state tomography, via the method described in [48].

D. Calibration

Since the phase shifter parameters (phase-per-electrical-power, and phase offset) varied between phase modulators, a calibration process was essential. Measuring the bright-light transmission from the inputs (IN and IN') to the outputs (OUT_T, OUT_B, OUT'_T, OUT'_B), we were able to characterise the electro-optic parameters of each thermal phase shifter, in a similar way to that described in [49]. We learned the parameters associated with each phase according to the scheme:

$$\begin{aligned}
\text{IN}' &\rightarrow \text{OUT}'_T, \text{OUT}'_B : \phi_B, \theta_{By1}, \theta_{CZB}, \theta_{Ty1}, \theta_{CZT} \\
\text{IN} &\rightarrow \text{OUT}'_T, \text{OUT}'_B : \phi_\beta, \phi_T, \theta_{Tz1}, \theta_{Bz1} \\
\text{IN} &\rightarrow \text{OUT}_T : \theta_{CZC}, \theta_{Ty2}, \theta_{Tz2}, \theta_{Tz3} \\
\text{IN} &\rightarrow \text{OUT}_B : \theta_{By2}, \theta_{Bz2}, \theta_{Bz3}.
\end{aligned} \tag{3}$$

We observed instabilities in the calibration data, due to changes in electrical contact resistance between our probe card and the on-chip gold pads. To mitigate this, we periodically recalibrated the on-chip parameters. Metallurgical wire-bonded contacts can prevent this in future. Low levels of thermal and common-ground crosstalk were observed but not compensated. Recent results suggest that crosstalk can be reduced through efficiency improvements, passive compensation methods, and by current driving of the thermal phase shifters [38, 49, 50].

The offsets of the tomographic z -rotation phases ($\theta_{Tz3}, \theta_{Bz3}$) were left at zero, meaning that additional random (fixed) z rotations were applied to each qubit before measurement. This choice was necessitated by the combined difficulty of: (1) calibrating the non-linear source phase

with bright light, and (2) doing this for each setting of the gate, in the device's finite stability time.

III. RESULTS

Source performance

One of the key metrics of a photon-pair source is its pair-generation efficiency [51]. This quantity is obtained from the photon-pair detection rate as a function of the input power, accounting for loss and detector efficiency. Inside the 1-nm-wide signal and idler spectral bands, we measured a brightness of 20 kHz/mW².

The indistinguishability between photon-pair sources is also important. The contrast of the RHOM block's quantum interference fringes indicates the indistinguishability of the block's constituent photon-pair sources. We measured RHOM quantum interference fringes on each source by configuring the chip to maximise photon flux at the OUT'_T and OUT'_B outputs, then varying ϕ_T and ϕ_B to obtain the fringes of Figure 2. We pumped the bottom source via the auxiliary input IN', and the top source via IN and the state-control MZI, integrating each point for 5 s. We observed $C = 93.2 \pm 1.4\%$ and $72.9 \pm 0.8\%$ fringe contrasts, respectively, for the top and bottom sources. Here, $C = (N_{\max} - N_{\min}) / (N_{\max} + N_{\min})$, where N_{\max} and N_{\min} are the accidental-subtracted maximum and minimum fitted count rates. The reduced contrasts can be explained by deviations (from the ideal $\eta = 50\%$) in the input evanescent couplers of each RHOM structure; they are compatible with reflectivity values of $\eta \approx 43\%$ and $\eta \approx 36\%$ for the top and bottom sources, respectively.

Quantum logic

We next quantified the device's control over entanglement. Quantum state tomography was used to extract the Purity ($P = \text{Tr}(\hat{\rho}^2)$ [41]), the CHSH param-

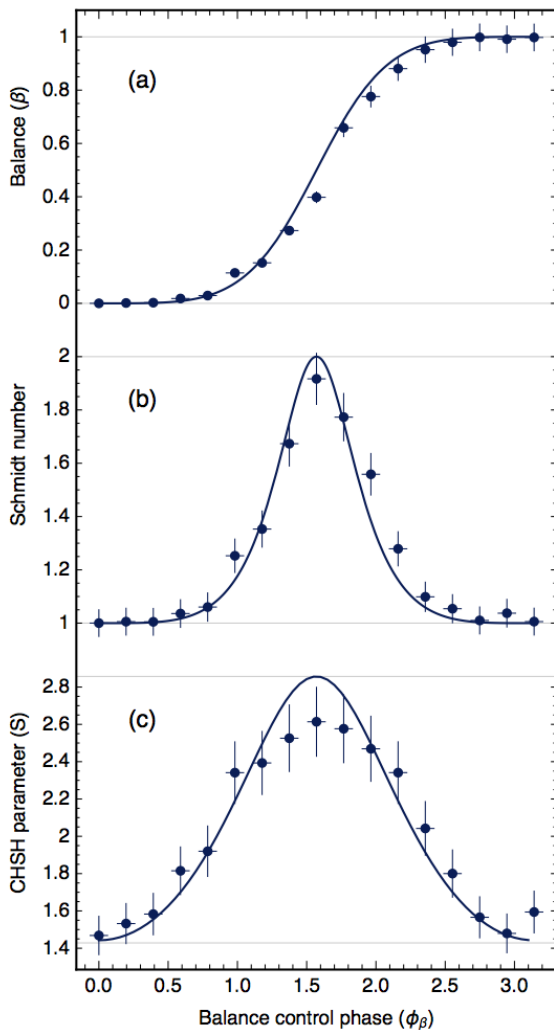


FIG. 3. Two-qubit state properties, direct from the source, as a function of the input state control phase, ϕ_β . **a** Balance between the $|00\rangle$ and the $|11\rangle$ components of the state, see equation (2). **b** Schmidt number. **c** CHSH parameter. Maximal entanglement occurs when the state is balanced, when $\phi_\beta = \pi/2$. Error bars were computed as one standard deviation of 200 trials around each tomographic measurement, each with a random sampling of Poisson photon noise. We assume a control phase uncertainty of $\pm\pi/50$.

ter, a strict measurement of quantum correlations, and the Schmidt number, analogous to the number of pure states represented in a given density matrix. These last two metrics show how separable the state is. The CHSH inequality, $S(\hat{\rho}) \leq 2$ [31, 42, 52], is violated when the state $\hat{\rho}$ cannot be represented by a local classical theory, indicating its entangled quantum nature. The Schmidt number, on the other hand, is an entanglement monotone and can give further evidence of the entangled or separable nature of $\hat{\rho}$ [42, 43, 53]. CHSH parameter values were obtained by computationally selecting an optimal measurement set for each of the states under analysis [31].

We analysed a wide set of separable and entangled

quantum states produced by the two-qubit source. Fixing $\phi_T = \phi_B = \pi/2$, we varied the phase of the state control MZI, ϕ_β , between 0 and π to prepare variably entangled states in the form of (1). When $\beta = 0$ or 1, separable states result, while when $\beta = 1/2$, a maximally entangled state is produced. States obtained directly from the source (bypassing the gate) showed good agreement with (1). These were measured using the OUT'_T and OUT'_B auxiliary outputs (see Figure 1b). Measured and calculated variations of the balance, Schmidt number, and CHSH parameter are plotted in Figure 3, versus the state control parameter ϕ_β .

In Figure 4 we show a sample of density matrices arising from the main device configurations, and we list their properties (purity, Schmidt number, CHSH parameter, and fidelity with the ideal z -rotated state) in Table I. Errors were obtained from Monte-Carlo simulations, based on 200 samples of Poissonian photon noise and accompanying tomographic reconstructions [54]. As expected, the \hat{I} -mode gate did not substantially affect the properties of the input states. The $\hat{C}z$ -mode gate, however, acted to entangle separable states, and separate entangled states, though it also degraded the purity. The limited contrast in the quantum interference of the two RHOM sources contributed to this reduction, by occasionally depositing two photons into one ‘qubit’. Gate and tomography calibration errors likely also contributed.

Since the entangling gate operates on the input state’s phase, we must examine with care the phase of the output state, $\arg[\hat{\rho}]$. The intrinsic and uncalibrated z -rotations on each qubit result in complicated phase pictures (Figure 4e,f). To compare these to their ideal counterparts, we computationally applied $\hat{R}_z(\zeta_t) \otimes \hat{R}_z(\zeta_b)$ to the reconstructed output state, and optimised the fidelity over local z -rotations via ζ_t and ζ_b . The resulting fidelities are listed in Table I and the process is shown visually in Figure 5.

DISCUSSION

We have presented a silicon-on-insulator quantum photonic device which embeds capabilities for the generation, manipulation, and analysis of two-qubit entangled states, by leveraging on-chip linear and non-linear optics. We showed how the device can prepare a variety of entangled and separable states, and operate on them using a switchable entangling gate. We demonstrated a new reconfigurable source of variably path-entangled non-degenerate photon pairs, using reversed Hong-Ou-Mandel quantum interference, and used on-chip quantum state tomography to measure its performance. The integration of this source with a complex integrated linear optical network enabled both the entanglement and disentanglement of the on-chip generated quantum states.

Device performance was hindered by imperfect beam-splitters and high coupling losses, leading to issues with stability, and ultimately limiting the measurable purity

and entanglement. However, the use of more advanced fibre couplers, such as those based on ultra-low loss gratings [55], together with adaptive methods, employing multiple imperfect MZIs for the realisation of a very high-quality one [34], can overcome these limitations, and enable high-performance, large-scale silicon photonic quantum devices in the near future.

ACKNOWLEDGEMENTS

We thank Damien Bonneau, Jianwei Wang, and Dylan Mahler for valuable discussions and support. We are grateful to Alasdair Price for help with preliminary characterisation. We also thank the staff of the James Watt Nano-fabrication Centre in Glasgow. We acknowledge support from the European Union through the BBOI, and from the QUCHIP projects. M.G. Thompson acknowledges support from an Engineering and Physical Sciences Research Council (EPSRC, UK) Early Career Fellowship and from the European Research

Council (ERC Grant Agreement number: 640079 QPE ERC-2014-ST). J.W. Silverstone acknowledges an EPSRC Doctoral Training Account, and a Natural Sciences and Engineering Research Council (Canada) Alexander Graham Bell Canada Graduate Scholarship. J.L.O'B. acknowledges a Royal Society Wolfson Merit Award and a Royal Academy of Engineering Chair in Emerging Technologies.

AUTHOR CONTRIBUTIONS STATEMENT

R.S. and J.W.S. contributed equally to this work. They conceived and designed the device, performed the experiments, and analysed the data. M.J.S. and M. Sorel fabricated the device. S.M., T.Y., M.F., M. Sasaki, and H.T. provided the superconducting detectors and M.G. Tanner, C.M.N., and R.H.H. built the detector system. M.G. Thompson supervised the work. All authors contributed to the manuscript.

-
- [1] Jeremy L. O'Brien, Akira Furusawa, and Jelena Vuckovic, "Photonic quantum technologies," *Nature Photonics* **3**, 687–695 (2009).
 - [2] Ludovico Latmiral, Niccolo Spagnolo, and Fabio Sciarrino, "Towards quantum supremacy with lossy scatter-shot boson sampling," *New Journal of Physics* **18**, 113008 (2016).
 - [3] Alberto Politi, Martin J. Cryan, John G. Rarity, Siyuan Yu, and Jeremy L. O'Brien, "Silica-on-silicon waveguide quantum circuits," *Science* **320**, 646–649 (2008).
 - [4] Benjamin J Metcalf, Justin B Spring, P C Humphreys, Nicholas Thomas-Peter, Marco Barbieri, W S Kolthammer, Xian-Min Jin, N K Langford, Dmytro Kundys, J C Gates, N J Smith, P G R Smith, and I A Walmsley, "Quantum teleportation on a photonic chip," *Nature Photonics* **8**, 770–774 (2014).
 - [5] Momchil Minkov and Vincenzo Savona, "A compact, integrated silicon device for the generation of spectrally filtered, pair-correlated photons," *Journal of Optics* **18**, 054012 (2016).
 - [6] Nobuyuki Matsuda, Peter Karkus, Hidetaka Nishi, Tai Tsuchizawa, W J Munro, Hiroki Takesue, and Koji Yamada, "On-chip generation and demultiplexing of quantum correlated photons using a silicon-silica monolithic photonic integration platform," *Optics Express* **22**, 22831–22840 (2014).
 - [7] Christian Reimer, Michael Kues, Lucia Caspani, Benjamin Wetzal, Piotr Roztock, Matteo Clerici, Yoann Jestin, Marcello Ferrera, Marco Peccianti, Alessia Pasquazi, Brent E Little, Sai T Chu, David J Moss, and Roberto Morandotti, "Cross-polarized photon-pair generation and bi-chromatically pumped optical parametric oscillation on a chip," *Nature Communications* **6**, 9236 (2015).
 - [8] Jacques Carolan, C Harrold, C Sparrow, E Martín-López, N J Russell, J W Silverstone, P J Shadbolt, N Matsuda, M Oguma, M Itoh, G D Marshall, M G Thompson, J C F Matthews, T Hashimoto, J L O'Brien, and A Laing, "Universal linear optics," *Science* **349**, 711–716 (2015).
 - [9] Linda Sansoni, Fabio Sciarrino, Giuseppe Vallone, Paolo Mataloni, Andrea Crespi, Roberta Ramponi, and Roberto Osellame, "Polarization entangled state measurement on a chip," *Physical Review Letters* **105**, 200503 (2010).
 - [10] Max Tillmann, Borivoje Dakic, René Heilmann, Stefan Nolte, Alexander Szameit, and Philip Walther, "Experimental boson sampling," *Science* **332**, 540–544 (2013).
 - [11] Fulvio Flamini, Lorenzo Magrini, Adil S Rab, Niccolò Spagnolo, Vincenzo D'Ambrosio, Paolo Mataloni, Fabio Sciarrino, Tommaso Zandrini, Andrea Crespi, Roberta Ramponi, and Roberto Osellame, "Thermally reconfigurable quantum photonic circuits at telecom wavelength by femtosecond laser micromachining," *Light Sci Appl* **4**, 354 (2015).
 - [12] Marco Bentivegna, Niccolo Spagnolo, Chiara Vitelli, Flavio Flamini, Niccolo Viggianiello, Ludovico Latmiral, Paolo Mataloni, D J Brod, E F Galvao, A Crespi, R Ramponi, R Osellame, and F Sciarrino, "Experimental scatter-shot boson sampling," *Science Advances* **1**, 1400255–1400255 (2015).
 - [13] Justin B Spring, Paolo L Mennea, Benjamin J Metcalf, P C Humphreys, J C Gates, Helen L Rogers, Christoph Söller, N J Smith, W S Kolthammer, P G R Smith, and I A Walmsley, "Chip-based array of near-identical, pure, heralded single-photon sources," *Optica* **4**, 90–96 (2017).
 - [14] Panagiotis Vergeris, Thomas Meany, Tommaso Lunghi, Gregory Sauder, James Downes, M J Steel, Michael J Withford, Olivier Alibart, and Sébastien Tanzilli, "On-chip generation of heralded photon-number states," *Scientific Reports* **6**, 1500 (2016).
 - [15] Olivier Alibart, Virginia D'Auria, Marc De Micheli, Florent Doutre, Florian Kaiser, Laurent Labonté, Tommaso

- Lunghi, Éric Picholle, and Sébastien Tanzilli, “Quantum photonics at telecom wavelengths based on lithium niobate waveguides,” *Journal of Optics* **18**, 104001 (2016).
- [16] Francesco Lenzini, Ben Haylock, Juan C. Loredó, Raphael A. Abraho, Nor A. Zakaria, Sachin Kasture, Isabelle Sagnes, Aristide Lemaitre, Hoang-Phuong Phan, Dzung Viet Dao, Pascale Senellart, Marcelo P. Almeida, Andrew G. White, and Mirko Lobino, “Active demultiplexing of single photons from a solid-state source,” *Laser and Photonics Reviews* **11**, 1600297 (2017).
- [17] Linda Sansoni, Kai Hong Luo, Christof Eigner, Raimund Ricken, Viktor Quiring, Harald Herrmann, and C Silberhorn, “A two-channel, spectrally degenerate polarization entangled source on chip,” *npj Quantum Information* **3**, 5 (2017).
- [18] Xiang Zhang, Yanbing Zhang, Chunle Xiong, and Benjamin J Eggleton, “Correlated photon pair generation in low-loss double-stripe silicon nitride waveguides,” *Journal of Optics* **18**, 074016 (2016).
- [19] David J Moss, Roberto Morandotti, Alexander L Gaeta, and Michal Lipson, “New CMOS-compatible platforms based on silicon nitride and Hydex for nonlinear optics,” *Nature Photonics* **7**, 597–607 (2013).
- [20] Joshua W. Silverstone, Damien Bonneau, Jeremy L. O’Brien, and Mark G. Thompson, “Silicon quantum photonics,” *IEEE Journal of Selected Topics in Quantum Electronics* **22**, 6700113 (2016).
- [21] J. E. Sharping, Kim F Lee, Mark A Foster, Amy C Turner, Bradley S Schmidt, Michal Lipson, Alexander L Gaeta, and P Kumar, “Generation of correlated photons in nanoscale silicon waveguides,” *Optics Express* **14**, 12388–12393 (2006).
- [22] Stefano Azzini, Davide Grassani, M J Strain, Marc Sorel, L G Helt, J E Sipe, Marco Liscidini, Matteo Galli, and Daniele Bajoni, “Ultra-low power generation of twin photons in a compact silicon ring resonator,” *Optics Express* **20**, 23100–23107 (2012).
- [23] Nobuyuki Matsuda, Hanna Le Jeannic, Hiroshi Fukuda, Tai Tsuchizawa, William John Munro, Kaoru Shimizu, Koji Yamada, Yasuhiro Tokura, and Hiroki Takesue, “A monolithically integrated polarization entangled photon pair source on a silicon chip,” *Scientific Reports* **2**, 00817 (2012).
- [24] Laurent Olislager, J Safioui, S Clemmen, K Phan Huy, W Bogaerts, R Baets, P Emplit, and S Massar, “Silicon-on-insulator integrated source of polarization-entangled photons,” *Optics Letters* **38**, 1960–1962 (2013).
- [25] M J Collins, C Xiong, I H Rey, T D Vo, J He, S Shahnian, C Reardon, T F Krauss, M J Steel, A S Clark, and B J Eggleton, “Integrated spatial multiplexing of heralded single-photon sources,” *Nature Communications* **4**, 2582 (2013).
- [26] Chunle Xiong, X Zhang, Z Liu, Matthew J Collins, A Mahendra, L G Helt, M J Steel, D Y Choi, C J Chae, P H W Leong, and B J Eggleton, “Active temporal multiplexing of indistinguishable heralded single photons,” *Nature Communications* **7**, 10853 (2016).
- [27] Kenichi Harada, Hiroki Takesue, Hiroshi Fukuda, Tai Tsuchizawa, Toshifumi Watanabe, Koji Yamada, Yasuhiro Tokura, and Sei-ichi Itabashi, “Indistinguishable photon pair generation using two independent silicon wire waveguides,” *New Journal of Physics* **13**, 065005 (2011).
- [28] J. W. Silverstone, D. Bonneau, K. Ohira, N Suzuki, H. Yoshida, N. Iizuka, M. Ezaki, C. M. Natarajan, M G Tanner, M. G. Tanner, R. H. Hadfield, V. Zwiller, G. D. Marshall, J G Rarity, J. L. O’Brien, and M. G. Thompson, “On-chip quantum interference between silicon photon-pair sources,” *Nature Photonics* **8**, 104–108 (2013).
- [29] Hiroki Takesue, Nobuyuki Matsuda, Eiichi Kuramochi, and Masaya Notomi, “Entangled photons from on-chip slow light,” *Scientific Reports* **4**, 448 (2014).
- [30] Xinan Xu, Zhenda Xie, Jiangjun Zheng, Junlin Liang, Tian Zhong, Mingbin Yu, Serdar Kocaman, Guo-Qiang Lo, Dim-Lee Kwong, Dirk R Englund, Franco N C Wong, and Chee Wei Wong, “Near-infrared Hong-Ou-Mandel interference on a silicon quantum photonic chip,” *Optics Express* **21**, 5014–5024 (2013).
- [31] J. W. Silverstone, R Santagati, D Bonneau, M J Strain, M Sorel, J L O’Brien, and M G. Thompson, “Qubit entanglement between ring-resonator photon-pair sources on a silicon chip,” *Nature Communications* **6**, 7948 (2015).
- [32] Nicholas C. Harris *et al.*, “Integrated source of spectrally filtered correlated photons for large-scale quantum photonic systems,” *Physical Review X* **4**, 041047 (2014).
- [33] Mateusz Piekarek, Damien Bonneau, S Miki, and T Yamashita, “High-extinction ratio integrated photonic filters for silicon quantum photonics,” *Optics Letters* **42**, 815 (2016).
- [34] C M Wilkes, X Qiang, J Wang, R Santagati, S Paesani, X Zhou, D A B Miller, G D Marshall, Mark G Thompson, and Jeremy L O’Brien, “60 dB high-extinction auto-configured Mach-Zehnder interferometer,” *Optics Letters* **41**, 5318–5321 (2016).
- [35] Faraz Najafi, Jacob Mower, Nicholas C Harris, Francesco Bellei, Andrew Dane, Catherine Lee, Xiaolong Hu, Prashanta Kharel, Francesco Marsili, Solomon Assefa, Karl K Berggren, and Dirk Englund, “On-chip detection of non-classical light by scalable integration of single-photon detectors,” *Nature Communications* **6**, 5873 (2015).
- [36] W H P Pernice, C Schuck, O Minaeva, M Li, G N Gol’tsman, and A V Sergienko, “High-speed and high-efficiency travelling wave single-photon detectors embedded in nanophotonic circuits,” *Nature Communications* **3**, 1325 (2012).
- [37] Qianfan Xu, David Fattal, and Raymond G Beausoleil, “Silicon microring resonators with 1.5- μm radius,” *Optics Express* **16**, 4309 (2008).
- [38] N C Harris, Y Ma, J Mower, Tom Baehr-Jones, D Englund, M Hochberg, and C Galland, “Efficient, compact and low loss thermo-optic phase shifter in silicon,” *Optics Express* **22**, 10487–10493 (2014).
- [39] Peter J Shadbolt *et al.*, “Generating, manipulating and measuring entanglement and mixture with a reconfigurable photonic circuit,” *Nat Photon* **6**, 45–49 (2012).
- [40] Jun Chen, Kim Fook Lee, and Prem Kumar, “Deterministic quantum splitter based on time-reversed Hong-Ou-Mandel interference,” *Physical Review A* **76**, 031804 (2007).
- [41] Omar Gamel and D F V James, “Measures of quantum state purity and classical degree of polarization,” *Physical Review A* **86**, 033830 (2012).
- [42] R. Horodecki, M. Horodecki, and K. Horodecki, “Quantum entanglement,” *Reviews of Modern Physics* **81**, 865–

- 942 (2009).
- [43] Barbara M Terhal and Pawel Horodecki, “Schmidt number for density matrices,” *Physical Review A* **61**, 040301 (2000).
 - [44] TC Ralph, N K Langford, T B Bell, and A G White, “Linear optical controlled-NOT gate in the coincidence basis,” *Physical Review A* **65**, 062324 (2002).
 - [45] P. D. Trinh, S. Yegnanarayanan, and B. Jalali, “Integrated optical directional couplers in silicon-on-insulator,” *Electronics Letters* **31**, 2097–2098 (1995).
 - [46] Shigehito Miki, Taro Yamashita, Hirotaka Terai, and Zhen Wang, “High performance fiber-coupled NbTiN superconducting nanowire single photon detectors with Gifford-McMahon cryocooler,” *Optics Express* **21**, 10208–10214 (2013).
 - [47] Juerg Leuthold, C. Koos, and W. Freude, “Nonlinear silicon photonics,” *Nature Photonics* **4**, 535–544 (2010).
 - [48] D F V James, P G Kwiat, W J Munro, and A G White, “Measurement of qubits,” *Physical Review A* **64**, 052312 (2001).
 - [49] Raffaele Santagati *et al.*, “Quantum simulation of hamiltonian spectra on a silicon chip,” eprint arXiv:1611.03511 (2016).
 - [50] S Paesani, A A Gentile, R Santagati, J. Wang, N Wiebe, D P Tew, J. L. O’Brien, and M. G. Thompson, “Experimental Bayesian Quantum Phase Estimation on a Silicon Photonic Chip,” *Physical Review Letters* **118**, 100503 (2017).
 - [51] M. Savanier, R. Kumar, and S. Mookherjea, “Photon pair generation from compact silicon microring resonators using microwatt-level pump powers,” *Optics Express* **24**, 3313–3328 (2016).
 - [52] Alain Aspect, Philippe Grangier, and Gérard Roger, “Experimental Realization of Einstein-Podolsky-Rosen-Bohm Gedankenexperiment: A New Violation of Bell’s Inequalities,” *Physical Review Letters* **49**, 91–94 (1982).
 - [53] J Sperling and W Vogel, “The Schmidt number as a universal entanglement measure,” *Physica Scripta* **83**, 045002 (2011).
 - [54] C F Roos, G P T Lancaster, M Riebe, H Häffner, W Hänsel, S Gulde, C Becher, J Eschner, F Schmidt-Kaler, and R Blatt, “Bell states of atoms with ultralong lifetimes and their tomographic state analysis,” *Physical Review Letters* **92**, 220402 (2004).
 - [55] Yunhong Ding, Haiyan Ou, and Christophe Peucheret, “Ultrahigh-efficiency apodized grating coupler using fully etched photonic crystals,” *Optics Letters* **38**, 2732–2734 (2013).

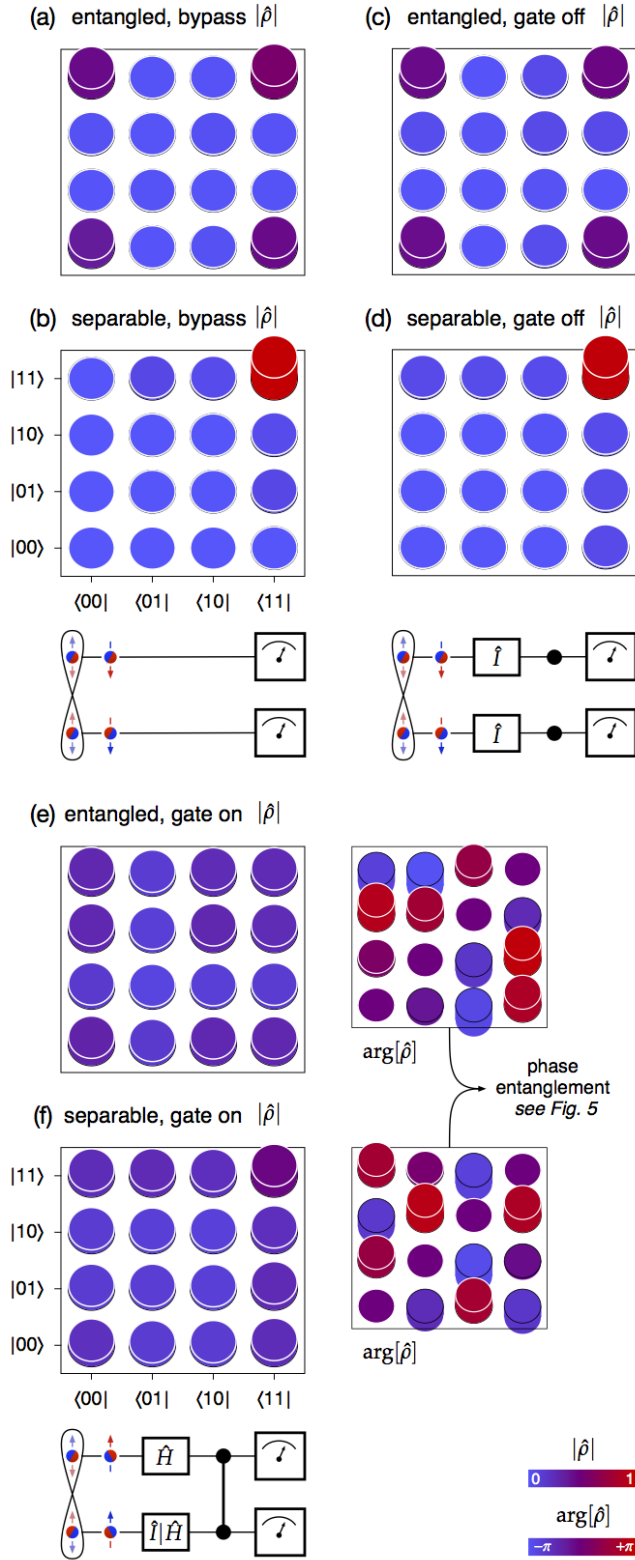


FIG. 4. Reconstructed output states for various source and gate configurations. States **a,c,e** are seeded by an entangled source state, while **b,d,f** are seeded by a $|11\rangle$ source state. States **a,b** bypass the gate; **c,d** pass through the gate set to \hat{I} ; and **e,f** pass through the gate set to $\hat{C}Z$, and include the phase information, below. State properties are compiled in Table I. Device configurations producing each set of states are shown at right.

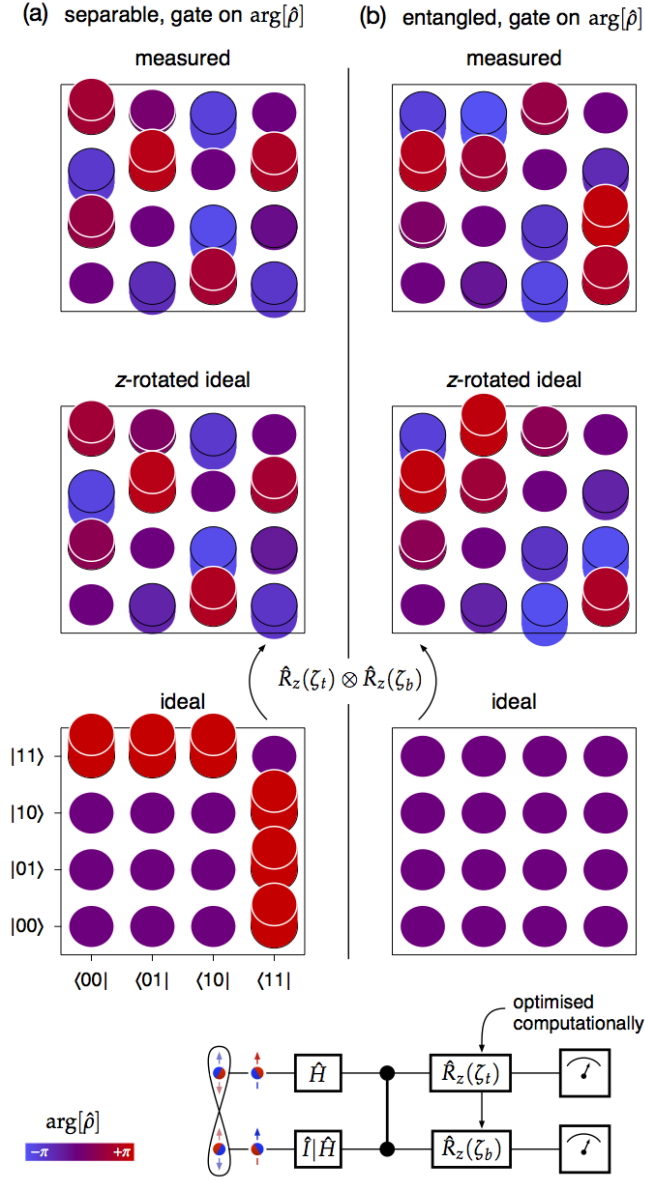


FIG. 5. Detail of phase entanglement, separability of states shown in Fig. Figure 4 e,f. Since the CZ gate operates on phase, random, fixed, local z -rotations obscure the underlying performance. The connection between the measured and ideal states, via numerical optimisation of ζ_t and ζ_b , is shown for **a** the gate-entangled, and **b** gate-disentangled states. In both cases the ideal density matrix magnitude is constant, $|\hat{\rho}_{i,j}| = 1/4$.